Disorder effects on the density of states of the II-VI semiconductor alloys Hg$_{0.5}$Cd$_{0.5}$Te, Cd$_{0.5}$Zn$_{0.5}$Te, and Hg$_{0.5}$Zn$_{0.5}$Te

Su-Huai Wei and Alex Zunger

Solar Energy Research Institute, Golden, Colorado 80401-3393

(Received 13 July 1990)

The electronic structure of substitutionally random $A_{1-x}B_xC$ alloys of zinc-blende semiconductors AC and BC departs from what a virtual-crystal approximation would grant both because of (i) a chemical perturbation, associated with an *electronic mismatch* between atoms A and B, and because of (ii) a structural perturbation (positional relaxation) induced by a *size mismatch* between A and B. Both effects on the electronic density of states are studied here for Hg$_{0.5}$Cd$_{0.5}$Te, Cd$_{0.5}$Zn$_{0.5}$Te, and Hg$_{0.5}$Zn$_{0.5}$Te in the context of first-principles self-consistent supercell models. We use our recently developed "special quasirandom structures" [A. Zunger, S.-H. Wei, L. G. Ferreira, and J. E. Bernard, Phys. Rev. Lett. **65**, 353 (1990)] concept whereby lattice sites of a periodic structure are occupied by A and B atoms so as to closely reproduce the structural correlation functions of an infinite, perfectly random alloy. Total-energy minimization provides then the relaxed atomic positions while application of the local-density formalism, as implemented by the linearized augmented-plane-wave method, describes self-consistently the consequences of chemical and structural perturbations. We show how these perturbations lead both to (i) distinct A-like and B-like features in the density of states and the electronic charge densities, and even to (ii) different C-like features associated with fluctuations in the local environments around the common sublattice.

I. INTRODUCTION

One of the central questions surrounding the physics of substitutionally disordered $A_{1-x}B_xC$ semiconductor alloys is the extent to which the local atomic structure and the various electronic states retain upon alloying their characteristics in the binary constituents. Early experiments[1-3] suggested that rather than view isovalent semiconductor alloys as new compounds in their own right, many of their properties can instead be usefully represented as a simple analytical interpolation between the properties P_{AC} and P_{BC} of the constituents

$$P(x) = [(1-x)P_{AC} + xP_{BC}] + b_P x(1-x) , \quad (1)$$

where b_P denotes the "bowing" in the quantity P. For example,[1-3] for P=lattice constant $b_a \sim 0$ (Vegard's rule),[4] for P=formation enthalpy (H), $b_H \sim 0$–0.1 eV/atom, for P=spin-orbit (SO) splitting $-b_{s.o.} \sim 0$–0.1 eV, and for P=direct band gap (g), $-b_g \sim 0$–3 eV. While the properties of ternary ABC_2, A_3BC_4, or AB_3C_4 compounds formed from strongly interacting constituents (e.g., *non-isovalent* chalcopyrites[5] such as CuGaSe$_2$ made of Cu$_2$S+Ga$_2$S$_3$) do not lend themselves to a simple description in terms of P_{AC} and P_{BC}, Eq. (1) does represent remarkably well many experimental observations[1-3] for a wide range of *isovalent* IV-IV, III-V, and II-VI semiconductor alloys. Indeed, much of the early experimental data on such alloys have substantiated the view that they represent "interpolative structures," e.g., (i) unlike glasses, amorphous semiconductors, or heavily doped systems, isovalent semiconductor alloys generally do not exhibit strong gap or "tail" states; instead, the alloy's optical spectra closely resembles that of the constituents with shifted (and somewhat broadened) peaks; (ii) diffraction patterns of such melt-grown alloys have the same symmetry as those of the constituent solids (with no extra spots); (iii) absorption and reflectance spectra are rather sharp, showing only modest alloy broadening of the near-edge transitions; and (iv) the principal Raman peaks shift smoothly with composition.

It is therefore understandable that early electronic-structure theories described such alloys in terms of weak, symmetry-preserving perturbations about the end-point constituents or their average. Indeed, such theories were *nonstructural,* in that they considered only the average occupations by $\langle A \rangle$ or $\langle B \rangle$ of *zinc-blende lattice sites,* removing the informational content associated with the *geometrical arrangements* of bonds around sites. Such is the virtual-crystal approximation[6] (VCA), where chemical identities of A and B are replaced by single, $\langle AB \rangle$ averaged atom in a fictitious crystal with the same space-group symmetry as the constituents, and so is the "site coherent-potential approximation"[7] (S-CPA), where the potential is modified relative to the VCA only on sites, and all A's and separately all B's are assumed equivalent and each is embedded in a uniform medium. In averaging atoms (VCA) or their environments (S-CPA), these site-only (i.e., "atomistic") theories described the electronic properties of the alloy through its topology, without specifying its actual geometry, i.e., the way in which the A—C and B—C bonds are arranged in space at a given composition x. These approaches have captured chemical trends among alloys insofar as even linear changes in volume or atomic pseudopotentials upon alloying produce nonlinear changes [Eq. (1)] in the electronic properties.

A closer look at the properties of isovalent semiconductor alloys, made possible by more recent measure-

ments[8-16] reveals, however, that the nonstructural theories do miss some qualitative features. It is obvious, for example, that the lower site symmetries of the A_3B, A_2B_2, and AB_3 clusters (C_{3v}, D_{2d}, and C_{3v}, respectively), which surround C atoms in fourfold coordinated $A_{1-x}B_xC$ alloys could produce effects which are absent in the higher (T_d) symmetry of the virtual $\langle AB \rangle_4$ cluster. Atomic displacements producing unequal A—C and B—C bond lengths[8] allowed only in the lower symmetries is just one such example. Simple symmetry-preserving nonstructural theories do not represent such distinct effects associated with the existence of a distribution of low symmetry environments; instead, it is assumed at the outset that the (configurational) average of a distribution of low symmetry configuration can be replaced by an "effective," high symmetry configuration. This can have significant implications on the description of optical[9] and structural properties. A few recent experimental observations are pertinent to this point.

(i) Extended x-ray-absorption fine-structure (EXAFS) experiments[8] on perfectly *random* (melt-grown, bulk) $A_{1-x}B_xC$ semiconductor alloys show that the actual (alloy-averaged) local structure about C is not tetrahedral, despite the fact that the constituents AC and BC are perfectly tetrahedral. Indeed, whereas the alloy's lattice constant $a(x)$ does represent, to within a good approximation, a linearly weighted average over the constituents [$b_a \sim 0$ in Eq. (1)], the A—C and B—C bond lengths do not average, but remain instead distinct and close to their values in the respective pure compounds for the entire composition range (Fig. 1). This behavior is summarized qualitatively in Table I.

(ii) $A_{1-x}B_xC$ alloys whose constituents are size mismatched can be ferroelectric,[10] e.g., $Cd_{1-x}Zn_xTe$. Clearly the site symmetry cannot be T_d, as the S-CPA or the VCA assume.

(iii) Nuclear magnetic resonance chemical shifts[11] $\sigma_C(A_nB_{4-n})$ of the common atom C, e.g., in $Cd_{1-x}Zn_xTe$ are resolvable into five components ($0 \leq n \leq 4$). These reflect distinct contributions by the five local atomic arrangements of the A and B atoms that are nearest neighbor to C. Similar results have been obtained for[12] $Hg_{1-x}Cd_xTe$.

(iv) The vibrational spectra of *homogeneous* random alloys are interpretable in terms of a superposition of frequencies characteristic of the distinct local clusters.[13,14] Furthermore, such alloys exhibit "no-phonon indirect transitions" which cannot be described by VCA. It can be explained by S-CPA only if the configuration average

was done after the matrix elements were calculated.[9]

(v) Averaging atoms produces, by construction, wave-function amplitudes which do not distinguish A from B. Yet photoemission studies,[15,16] clearly resolve A-type from B-type valence-band states in isovalent $A_{1-x}B_xC$ semiconductor alloys. These can be described by the S-CPA, but not by the VCA.

All of the features noted above have been observed in (melt-grown) nearly perfectly random homogeneous semiconductor alloy samples, having no significant short- or long-range order. It is hence becoming clear that on the coherence length scale of the valence electrons, the "personalities" of atoms, bonds, and tetrahedra might survive alloy averaging and that random alloys possess a significant structure on this scale.

In the present work we study the extent to which characteristic features in the electronic structure and density of states of II-VI zinc-blende-structure tellurides

Bond Type	Length in Binaries	Length in x=1/2 Alloy

(a) $Cd_{1-x}Zn_xTe$

Cd-Te   2.806Å   2.795Å

$\bar{R}$ 2.721Å

Zn-Te   2.637Å   2.655Å

(b) $Hg_{1-x}Zn_xTe$

Hg-Te   2.798Å   2.783Å

$\bar{R}$ 2.717Å

Zn-Te   2.637Å   2.655Å

FIG. 1. Calculated changes (see Sec. V A) in nearest-neighbor bond lengths (in Å) upon formation of the 50–50 % alloys. (a) $Cd_{0.5}Zn_{0.5}Te$, (b) $Hg_{0.5}Zn_{0.5}Te$. The LDA-calculated values for the binary compounds have been scaled in this figure to the experimental values. $\bar{R}$ denotes the average.

TABLE I. Qualitative trends in molar volumes and nearest-neighbor bond lengths upon formation of a tetrahedrally coordinated alloy with size-mismatched constituents (see Fig. 1). The changes in molar volume and bond lengths are given with respect to the values in the binary semiconductors and the VCA, respectively.

	Cd-Zn-Te or Hg-Zn-Te alloys	
	ZnTe component	CdTe or HgTe component
Molar volume with respect to binaries	Larger	Smaller
Bond lengths with respect to $\bar{R}$	Shorter	Longer
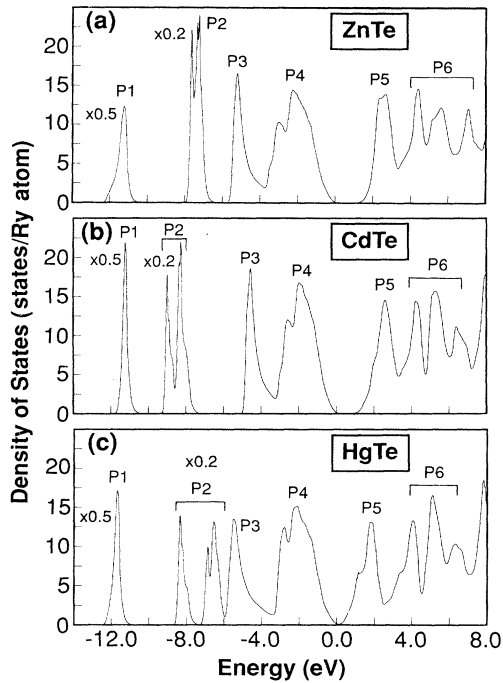
FIG. 2. Total DOS of (a) ZnTe, (b) CdTe, and (c) HgTe, evaluated at their respective zinc-blende equilibrium lattice constants. Peaks at different regions are labeled as $P1$–$P6$. Notice the change of scale for the $P1$ and $P2$ peaks. Zero of energy is at the VBM.

are retained in a perfectly random alloy. We will use a *structural* theory for such alloys, hence permitting the electronic states of the binary constituents to either "mix" or "separate" upon alloying, depending on the nature of the individual states and their interactions. To help formulate more precisely the questions which we address (Sec. III), we first describe the characteristic electronic states in zinc-blende-structure II-VI tellurides.

II. ELECTRONIC STATES IN II-VI ZINC-BLENDE-STRUCTURE TELLURIDES

The electronic structure of the II-VI semiconductors studied here were calculated within the local-density approximation[17] (LDA) as implemented by the first-principles linearized augmented-plane-wave (LAPW) method,[18] using the Hedin-Lundqvist exchange correlation.[19] The equilibrium structural parameters were obtained through the minimization of total energy and were given previously.[20] To converge the electronic charge density and the total energy we use two special k points[21] in the irreducible Brillouin zone of the zinc-blende (ZB) structure and about 200 basis functions per ZB unit cell. The muffin-tin radii used are 2.3532, 2.6193, 2.6193, and 2.5137 bohrs for Zn, Cd, Hg, and Te, respectively. The convergence error in the alloy formation energy is ~5 meV/4 atoms. The density of states (DOS) was calculated using the tetrahedron integration method[22] with a uniform mesh of 512 k points in the ZB Brillouin zone. The
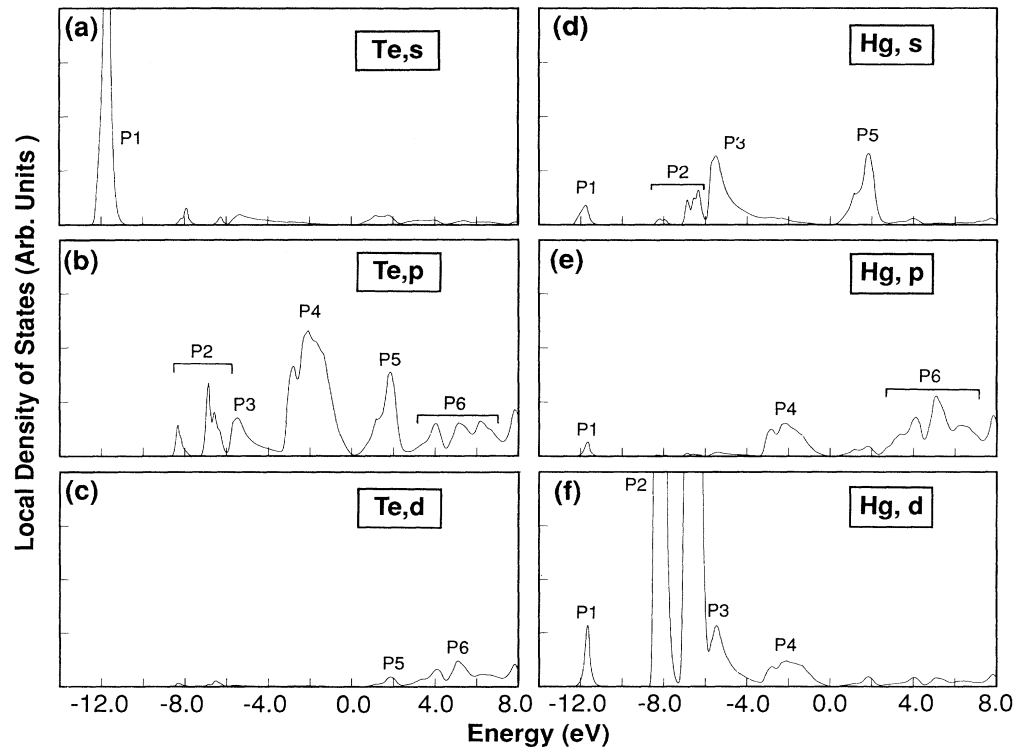
FIG. 3. Site and angular momentum projected local density of states (LDOS) for HgTe. Notice that the absolute values of the LDOS are arbitrary as they depend on the choice of the sphere radii used for integration. The radii used are given in Sec. II. Zero of energy is at the VBM.
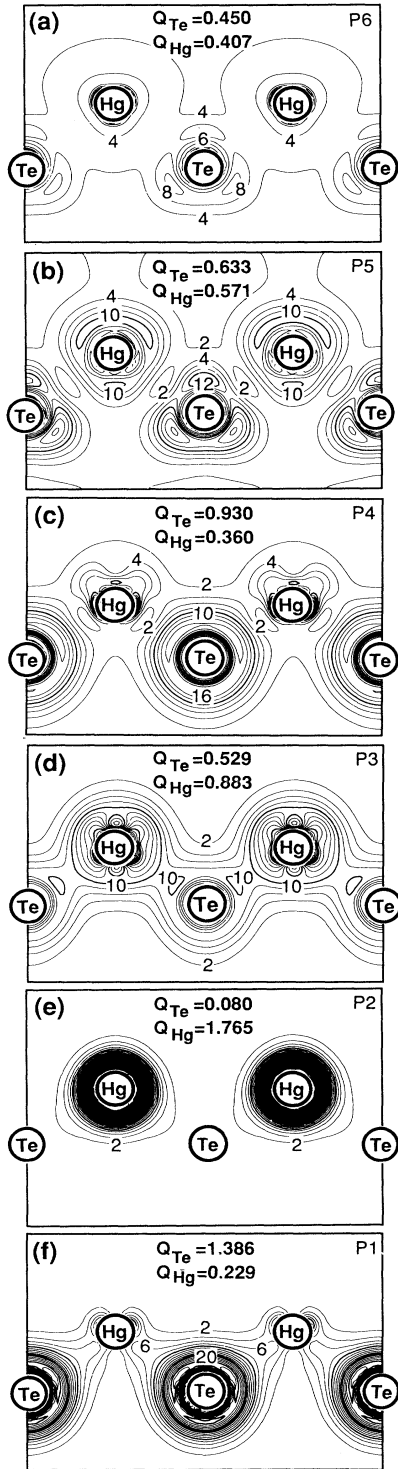
FIG. 4. Electronic charge-density contour plots for the various DOS peaks $P1-P6$ of HgTe [defined in Fig. 2(c)]. The charge density shown in each panel is renormalized to $2e$ per zinc-blende unit cell. The contour step size is 2×10^{-3} e/a.u.^{3} We also give for each panel the total integrated charge inside the muffin-tin spheres with radii of 2.6512 bohrs for both Te and Hg.

DOS was broadened using a Gaussian-like function with full width at half maximum (FWHM) equal to 0.2 eV (unbroadened DOS are given for comparison; e.g., Fig. 10 below). Full relativistic effects, including spin-orbit interaction through a second variation procedure,[23] were included.

LDA eigenvalues are known[24] to underestimate the true quasiparticle binding energies, in particular, for highly localized states. For example, the calculated cation d orbital energies (relative to valence-band maximum) in the d^{10} configuration in II-VI semiconductors are too high[20] by about 2 eV when compared with the observed d^{10}/d^9 photoemission energies.[25] The error is considerably smaller for extended states. This discrepancy originates both from the neglect of core-hole relaxation[26] and from distinct many-body corrections.[27,28] However, the calculated spin-orbit splittings[20] of the d orbitals agree with experimental value[25] to within 0.1 eV. Since we focus in this work mostly on the alloy-induced *shifts* in particular zinc-blende states (rather than on absolute binding energies), our results will not be sensitive to the LDA errors.

Figure 2 depicts the calculated total density of states for the zinc-blende structure tellurides ZnTe, CdTe, and HgTe. They exhibit a number of distinct features in the valence (denoted $P1-P4$) and lowest conduction (denoted $P5,P6$) bands. To analyze these states, we have calculated for each of these three compounds the site and angular momentum projected local density of states (LDOS), as well as the electronic charge density enclosed within each of the DOS peaks. These LDOS and charge densities are illustrated for HgTe in Figs. 3 and 4, respectively (the results for ZnTe and CdTe are qualitatively similar). This analysis is then used to identify the orbital character and localization of distinct "generic" zinc-blende states as shown in Table II. We see that the II-VI tellurides exhibit (i) *atom-centered localized states*, such as the Te and s states denoted $P1$ and the spin-orbit split metal d bands denoted $P2$; (ii) *bond-centered localized states* such as the sp^3 bonding $P3$ state and its $P5$ antibonding counterpart; the electronic charge density is localized in the bond and antibond directions, respectively; and (iii) *volume-extended states* which have amplitude both on atomic sites and in the interstitial regions, e.g., the $P4$ and $P6$ states. Notice that substantial metal d character exists[20] (in particular for HgTe) in the $P1$, $P3$, and $P4$ states [Fig. 3(f)].

TABLE II. Main orbital character of the peaks in the density of states of the II-V tellurides (see Figs. 3 and 4). Here M denotes metal atoms (Zn,Cd,Hg).

DOS peak	Majority character	Localization
$P1$	Te,s	on Te
$P2$	M,d	on M
$P3$	Te,p + M,s	on M—Te bond
$P4$	Te,p + M,p	extended + Te bond
$P5$	Te,p + M,s	on M-Te antibond
$P6$	M,p + Te,p	extended + Te antibond

III. QUALITATIVE DISCUSSION OF POSSIBLE ALLOY EFFECTS ON ZINC-BLENDE STATES

The different types of zinc-blende states (Table II) might respond differently to alloying: they can appear in the alloy either as "split bands" or as "mixed," broadened bands, depending on their energy separation in the constituents on the scale of the interband coupling in the alloy. We have seen that alloys whose constituents are size mismatched ($Cd_{1-x}Zn_xTe$ and $Hg_{1-x}Zn_xTe$) exhibit changes both in the partial molar volumes and bond lengths (Fig. 1 and Table I). We expect then that relative to the more extended states ($P4, P6$) the energies of atom-centered localized states ($P1, P2$) will be modified by the changed volume (a hydrostatic pressure effect) while bond centered localized states ($P3, P5$) will respond primarily to the changed bond lengths (a strain effect). Examination of the changes in volume and bond length upon alloying seen in x-ray[8] and EXAFS (Ref. 8) measurements, respectively, along with typical values of hydrostatic and phonon deformation potentials in semiconductors[3,29] suggest that the corresponding level shifts can be up to a few tenths of an eV. Note from Table I that these changes have *opposite signs*, e.g., in $Cd_{1-x}Zn_xTe$ the ZnTe (CdTe) partial molar volumes are increased (decreased) with respect to the binaries at equilibrium. The attendant hydrostatic effect in the alloy could then shift the atom-centered bonding states to lower (higher) binding energies, depending on whether the alloy wave function is localized on ZnTe or CdTe, respectively. Similar remarks pertain to strain-induced shifts: Table I and Fig. 1 show that in $Cd_{1-x}Zn_xTe$ for example, the Zn—Te (Cd—Te) bond becomes shorter (longer) relative to the VCA average (denoted $\bar{R}$ in Fig. 1). Hence bond-centered bonding states (e.g., $P3$) could shift to lower (higher) energies upon structural relaxation, leading possibly to new alloy behavior relative to the VCA or the S-CPA. In alloys whose constituents are nearly size matched ($Hg_{1-x}Cd_xTe$) there are no such relaxation effects; it is just the chemical disparity between the unperturbed zinc-blende states which controls the alloy behavior. For example, the substantial difference between the Hg and Cd atomic s orbital energies (~ 1.2 eV) (Ref. 20) is reflected by a similar shift in the energies of the zinc-blende states having large metal s character [$P3$ and $P5$; see Figs. 2(b) and 2(c)]; if alloy coupling is weak, this large separation could lead to a split-band behavior in the alloy.

We have discussed so far the way in which chemical and structural differences in the *mixed* A-B sublattice in $A_{1-x}B_xC$ could lead to different alloy behaviors. These differences are averaged out in the VCA (which is incapable, therefore, of exhibiting a split-band behavior), whereas the chemical effect is retained to low order in the S-CPA. Fluctuations could exist, however, also in the *common* sublattice C. While in a pure tetrahedral compound AC there is but a *single* (repeated) local environment consisting of an A_4 tetrahedron centered about C, an $A_{1-x}B_xC$ alloy exhibits a *distribution* of local environments, e.g., C-centered tetrahedra of the type A_4,

A_3B, A_2B_2, AB_3, and B_4. The VCA idealized this situation by using a single $\langle AB \rangle_4$ tetrahedron whose properties (molar volumes and potential) are scaled relative to the end-point constituents. The standard CPA approach recognizes only atomic sites (not tetrahedra), hence it assumes that at each composition there is but a single type of C atom (this limitation could be lifted, at the expense of greater computational complexity, by assigning different diagonal energies to different atoms of the same chemical identity). In reality, the different site symmetries and electronegativities of the five C-centered $A_{4-n}B_n$ ($0 \leq n \leq 4$) tetrahedra could affect the nature of the alloy states associated with the C atom. This is evident, among others, from the existence of distinct NMR chemical shifts for the five types of C atoms,[11,12] from distinct phonon states for difference clusters,[13,14] and from statistical thermodynamic calculations for such alloys.[30]

This qualitative discussion focuses the issues to be analyzed below: we will follow the evolution of the characteristic zinc-blende features $P1$–$P6$ (Figs. 2–4) in the respective random alloys, examining the way in which the chemical perturbations as well as structural relaxations affect the emerging alloy states.

IV. STRUCTURAL MODELS FOR RANDOM ALLOYS

Our foregoing discussion suggests that a realistic model for the structure of a perfect random substitutional alloy should categorize it not just in terms of a random distribution of *sites*, but also in terms of a distribution of larger clusters, e.g., bonds, tetrahedra, etc. A number of previous attempts have been made at improving the S-CPA in this light, including the introduction of off-diagonal disorder,[31] molecular CPA (M-CPA),[32] the traveling-cluster approximation,[33] or through the "next-neighbor CPA,"[34] etc. The complexity of such models, however, has not been conducive to the use of first-principles electronic Hamiltonians that permit full charge self consistency, introduction of general atomic relaxations, large basis sets, and explicit electron-electron (Coulomb, exchange, and correlation) interactions.

A direct approach to constructing a structural model for substitutional random alloys would involve the definition of a sufficiently large-N atoms per cell (periodic supercell whose sites are occupied at random by either A or B; the atomic positions would then be relaxed (without interchanging atoms) to minimize the total energy. At the statistical, large-N limit, even a single configuration would manifest (by ergodicity) all possible local environments. Solving for the electronic spectral functions of such structures would then provide a model for the alloy's electronic properties. In practice, only $O(10^3)$ atoms per cell or less were considered in such models.[35-37] Since this is nevertheless a large number as far as electronic structure theory is concerned, by necessity, the electronic structure was often described within highly simplified electronic Hamiltonians (e.g., non-self-consistent, minimal-basis-set tight-binding models solved through recursion methods[35]). This direct approach has nevertheless yielded "benchmark results," against which

more approximate methods such as S-CPA were tested. The approximations involved in the electronic Hamiltonian prevented the introduction of atomic relaxations or self-consistent charge transfer. Far smaller supercells (~ 50 atoms per cell) are required if the current first-principles method of electronic structure were to be applied to such supercell models. Using the standard approach of occupying each site at random by A or B, such smaller supercells could depart significantly from the statistical limit of random networks.[38]

A more effective method can be based on careful selection of smaller supercells that mimic the properties of large cells with random occupation of sites. The extent to which a given configuration σ of A and B atoms in a supercell with N sites approaches the limit of a perfectly random infinite network can be measured by its structural correlation functions.[38] Here one assigns a fictitious spin variable $\hat{S}_i$ to each site i; it takes the value -1 if i is occupied by A and $+1$ if occupied by B. One then discretizes configuration σ into a set of "figures" $\{f\}$ consisting of atom clusters with k vertices, separated by up to the mth neighbor. For example, the figure $(k,m)=(2,m)$ represents pairs of atoms that are m neighbors apart, the figure $(k,m)=(3,1)$ represents nearest-neighbor triangles, and $(k,m)=(4,1)$ gives a tetrahedron whose atoms are nearest neighbors to one another. (In the present notation, first fcc A-B neighbors are equal to second neighbors in the zinc-blende structure.) The "empty figure" is labeled, by convention, as $(k,m)=(0,1)$. Note that in the S-CPA, one counts only the figures $(k,m)=(1,0)$, i.e., single-site figures.

We define for configuration σ the multisite spin product

$$\Pi_f(\sigma) = \prod_i \hat{S}_i(\sigma) \, , \qquad (2)$$

taken over all vertices of figure $f=(k,m)$. There are $D_{k,m}$ equivalent figures per site. For an ordered periodic structure $\sigma = S$ we will take the lattice-averaged product (denoted by an overbar) $\overline{\Pi}_f(S)$ over all symmetry-equivalent figures in the lattice. While for a particular (ordered) structure S we have a distinct set $\{\overline{\Pi}_f(S)\}$ which defines this structure, in a binary random (R) alloy we must take the configurational average (denoted by angular brackets) over all 2^N structures $\{\sigma\}$. The result is known analytically:

$$\langle \overline{\Pi}_{k,m} \rangle_R = (2x-1)^k \, , \qquad (3)$$

so that at $x=\frac{1}{2}$, for example, all correlation functions vanish, except $\langle \overline{\Pi}_{0,1} \rangle = 1$.

Standard approaches for constructing models for random substitutional networks[35−37] attempt to approach the statistical limit of Eq. (3) using a site-by-site occupation of the N lattice site; this approaches the statistical limit as slowly as $N^{-1/2}$, leading to large errors[38] for supercells that are small enough to be currently treated by first-principles electronic Hamiltonians. We assume now that there exists a natural hierarchy of figures, whereby

figures whose atoms are separated by large distances exhibit weaker interactions than those in which atoms are closer to one another. It is then possible to ask whether there exists a "special" arrangement of N atoms in a periodic supercell so that its distinct set $\{\overline{\Pi}_{k,m}(S)\}$ best matches the configurationally averaged correlation functions $\{\langle \Pi_{k,m} \rangle_R\}$ of an infinite, perfectly random network for the first few (most significant) figures (k,m). We refer to these as "special quasirandom structures" (SQS's). We have previously shown[38,39] that, e.g., at $x=\frac{1}{2}$ in fcc lattices such SQS's exist already for $N=4$ (denoted SQS-4) and $N=8$ (SQS-8); they reproduce with only small errors the first few (pair as well as many-body) correlation functions of the random alloy far better than the site-by-site (coin-flip) occupation scheme. We find that SQS-4 is an $(AC)_2(BC)_2$ superlattice whose AC and BC layers repeat along the [110] direction, whereas SQS-8 is an $(AC)_2(BC)_3(AC)_2(BC)_1$ (or its variant with $A \leftrightarrow B$ replacement) superlattice along the [113] direction. SQS-4 and SQS-8 have, respectively, four and eight mixed A,B atoms per cell or a total of eight and sixteen atoms per cell (counting also the common sublattice C). Note that unlike the case in the VCA and the S-CPA, all the C atoms as well as all A atoms (and separately all B atoms) could be crystallographically inequivalent in these SQS's, hence these structures exhibit a distribution of local environments such as inequivalent sites, bonds, and tetrahedra.

To the extent that a SQS-N mimics the configurationally averaged structure of a random alloy (through matching of the $\overline{\Pi}_f$'s), so would its electronic properties. Since, however, a SQS-N with small N does contain some errors $|\overline{\Pi}_{k,m}(\text{SQS}) - \langle \overline{\Pi}_{k,m} \rangle_R| \neq 0$ in its correlation functions, it is important to check how these errors affect the calculated electronic properties. The test done to date were described elsewhere;[39,40] they are summarized briefly here.

(i) A ~ 2300 atom per cell random configuration of the $Al_{0.5}Ga_{0.5}As$ alloy was generated[40] through site-by-site occupation and subjected to a tight-binding Hamiltonian solved by the recursion method. The same Hamiltonian was separately applied to the 16-atom SQS-8 model. The two calculations yield Γ_{15v}-Γ_{1c}, Γ_{15v}-X_{1c}, Γ_{15v}-X_{3c}, and Γ_{15v}-L_{1c} band gaps (typically around ~ 2 eV) which are within 0.02 eV or less from each other. The SQS calculation reproduces also very well the distribution of states, as measured by the second moment of the spectral functions at various wave vectors in the zinc-blende Brillouin zone.

(ii) A single total-energy calculation on either SQS-4 or SQS-8 reproduces closely the mixing enthalpy of the random alloy as calculated by summing over the contributions (k,m) of pair interactions (up to $m=6$), as well as the first few three-body and four-body terms.[38,39]

(iii) Minimization of the total elastic energy of ~ 1000-atom supercells of $Si_{0.5}Ge_{0.5}$ and averaging over a sufficient number of random configurations produces total elastic energies that are within 0.2 meV/atom of what a single, eight-atom SQS gives.[39(c)] In what follows, we apply the SQS concept to study the electronic structure of the II-VI telluride alloys.

V. TOTAL ENERGIES, EQUILIBRIUM STRUCTURES, AND BAND GAPS

A. Structure of the SQS-N

In the present work we study the total energies and density of states of $Cd_{0.5}Zn_{0.5}Te$, $Hg_{0.5}Zn_{0.5}Te$, and $Hg_{0.5}Cd_{0.5}Te$ using the SQS-4 model. The predictions of the SQS-4 model were also tested against the more accurate SQS-8 model in some cases.

The SQS-4 structure [Fig. 5(a)] has the space group C_{2v}^7 ($Pmn2_1$) with primitive orthorhombic unit cell vectors

$$\mathbf{a} = (-\tfrac{1}{2}, \tfrac{1}{2}, 0)\eta a \ ,$$

$$\mathbf{b} = (0, 0, 1)a \ ,$$ (4)

$$\mathbf{c} = (1, 1, 0)\xi a \ .$$

The atomic positions (in Cartesian coordinates) take the general forms

$$\tau_{i,1} = [\xi x_i; \xi x_i; z_i]a \ ,$$

$$\tau_{i,2} = [-\eta/4 - \xi x_i; \eta/4 - \xi x_i; \tfrac{1}{2} + z_i]a \ ,$$ (5)

where $i = 1, 2, 3,$ and 4 corresponds to occupation by A, B, C, and C, respectively. In the macroscopic random alloy (infinite supercell size) there is no unique crystallographic direction. We mimic this in the finite SQS-N by setting the cell external parameters to its ideal values ($\xi = \eta = 1$ for SQS-4). This is further supported by our total-energy calculations[30] for ordered compounds, where we find that, despite the long-range order, the noncubic distortion in the isovalent A,B sublattice is less than 1%. The dimensionless cell-internal parameters x_i and z_i represent the structural degrees of freedom that are not determined by symmetry; they need to be relaxed to achieve a minimum in the total energy given the cell external vectors ($\mathbf{a}, \mathbf{b}, \mathbf{c}$). In the *unrelaxed* structure the cell internal parameters take the "ideal" zinc-blende values

$$x_1 = -\tfrac{1}{8}, \quad z_1 = 0 \quad (A) \ ;$$

$$x_2 = \tfrac{3}{8}, \quad z_2 = 0 \quad (B) \ ;$$ (6)

$$x_3 = \tfrac{1}{8}, \quad z_3 = \tfrac{1}{4} \quad (C) \ ;$$

$$x_4 = -\tfrac{3}{8}, \quad z_4 = \tfrac{1}{4} \quad (C)$$

that lead to *equal* nearest-neighbor bond lengths

$$\bar{R}(x) = R_{AC} = R_{BC} = \sqrt{3}/4a(x) \ ,$$ (7)

in contrast with experiment.[8] This highlights the need for relaxation.

The SQS-8 structure [Fig. 5(b)] has the space group C_s^3 with the monoclinic unit cell vectors

$$\mathbf{a} = (1, \tfrac{1}{2}, -\tfrac{1}{2})a \ ,$$

$$\mathbf{b} = (\tfrac{1}{2}, -\tfrac{1}{2}, 0)a \ ,$$ (8)

$$\mathbf{c} = (1, 1, 2)a \ .$$

As argued in the above, we have taken the ideal values in Eq. (8) for the cell external parameters. The atomic positions (in Cartesian coordinates) take the general form ($i = 1$–16)

$$\tau_i = [x_i, x_i, z_i]a \ .$$ (9)

For the unrelaxed structure the cell internal parameters x_i and z_i take the "ideal" values

$$x_1 = 0, \quad z_1 = 0 \quad (A) \ ;$$

$$x_2 = \tfrac{1}{2}, \quad z_2 = 0 \quad (A) \ ;$$

$$x_3 = -\tfrac{1}{2}, \quad z_3 = 2 \quad (A) \ ;$$

$$x_4 = 0, \quad z_4 = 2 \quad (A) \ ;$$

$$x_5 = 0, \quad z_5 = 1 \quad (B) \ ;$$

$$x_6 = \tfrac{1}{2}, \quad z_6 = 1 \quad (B) \ ;$$

$$x_7 = -\tfrac{1}{2}, \quad z_7 = 1 \quad (B) \ ;$$

$$x_8 = \tfrac{1}{2}, \quad z_8 = 2 \quad (B) \ ;$$

$$x_9 = \tfrac{1}{4}, \quad z_9 = \tfrac{1}{4}(C) \ ;$$ (10)

$$x_{10} = \tfrac{3}{4}, \quad z_{10} = \tfrac{1}{4} \quad (C) \ ;$$

$$x_{11} = -\tfrac{1}{4}, \quad z_{11} = \tfrac{5}{4} \quad (C) \ ;$$

$$x_{12} = \tfrac{1}{4}, \quad z_{12} = \tfrac{5}{4} \quad (C) \ ;$$

$$x_{13} = \tfrac{3}{4}, \quad z_{13} = \tfrac{5}{4} \quad (C) \ ;$$

$$x_{14} = -\tfrac{1}{4}, \quad z_{14} = \tfrac{9}{4} \quad (C) \ ;$$

$$x_{15} = \tfrac{1}{4}, \quad z_{15} = \tfrac{9}{4} \quad (C) \ ;$$

$$x_{16} = \tfrac{3}{4}, \quad z_{16} = \tfrac{9}{4} \quad (C) \ .$$

Note that the SQS-8 structure has two variants, obtained by switching the A and B atoms. They differ only in the rather small, three-body $\overline{\Pi}_{3,m}$ correlation functions and yield essentially identical total energies (within 2 meV/4-
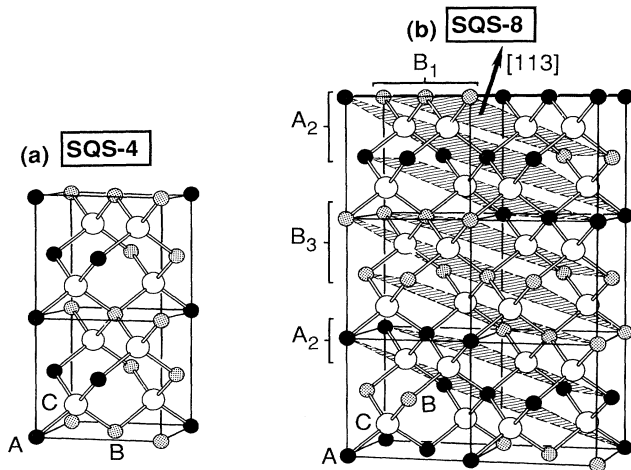
FIG. 5. Crystal structure of the special quasirandom structures (SQS) of the type (a) SQS-4 and (b) SQS-8 for the $x = \tfrac{1}{2}$ alloy.

atoms). In a proper calculation, however, the results for both structures should be averaged. This average (giving $\overline{\Pi}_{3,m}=0$) contains all five possible nearest-neighbor (C-centered) tetrahedra A_4, A_3B, A_2B_2, AB_3, and B_4 in the ratio 1:4:6:4:1 as required by the random (Bernoulli) distribution at $x=\frac{1}{2}$. We will see below (Sec. VI C) that SQS-8 calculations of the density of states often reflect contributions of such tetrahedra in this ratio.

The equilibrium atomic positions in the SQS model are obtained by minimizing the total energy with respect to the cell internal coordinates of Eq. (5), subject to a fixed cubic lattice constant a in Eq. (4) taken as the average of the LAPW calculated values of the zinc-blende constituents (this Vegard's rule is satisfied closely by most isovalent semiconductor alloys[1]). To aid this multiparameter optimization we use Keating's valence-force-field[41] (VFF) model with bond-bending and bond-stretching force constants tabulated in Ref. 42, and equilibrium bond lengths obtained from the LAPW calculations on the binary constituents,[20] i.e.,

$$R(\text{Zn—Te})=2.621 \text{ Å} ,$$

$$R(\text{Cd—Te})=2.802 \text{ Å} , \qquad (11)$$

$$R(\text{Hg—Te})=2.811 \text{ Å} .$$

Optimizing the structure with this modified VFF provides an excellent guess to the equilibrium geometry. The VFF results are then verified by the LAPW total energy calculations and found, in most cases, to be very close. The resulting equilibrium structural parameters are given in Table III; the resulting bond lengths are compared in Fig. 1 to a virtual-crystal average and to the values in the binary constituents. In this figure we have used a normalization factor $v=a_{eq}^{\text{expt}}/a_{eq}^{\text{LDA}}$ to scale the calculated LDA bond lengths of the pure zinc-blende constituents to the experimental (expt.) values. The values obtained in this way for the $Cd_{0.5}Zn_{0.5}Te$ alloy $R(\text{Zn—Te})=2.655$ Å and $R(\text{Cd–Te})=2.795$ Å compare very well with the EXAFS measurements of Motta et al.[8(b)] [$R(\text{Zn—Te})=2.659$ Å and $R(\text{Cd—Te})=2.790$ Å]. They deviate significantly from the VCA value at $x=\frac{1}{2}$ of Eq. (7), i.e., $\overline{R}=2.721$ Å. This deviation (generally larger in II-VI systems than in III-V alloys because of the smaller bond-bending force constant in the former) indicates that the system has used its cell-internal structure degrees of freedom to reduce the strain energy. This has significant effects on the thermodynamic properties[30] as well as on the electronic structure of the alloy (see

below). For $Hg_{0.5}Zn_{0.5}Te$ we find similar agreement between the calculated alloys bond lengths [$R(\text{Zn—Te})=2.655$ Å and $R(\text{Hg—Te})=2.783$ Å] and the EXAFS measurements[8(c)] [$R(\text{Zn—Te})=2.643$ Å and $R(\text{Hg—Te})=2.796$ Å]. Because of the small lattice mismatch in $Hg_{1-x}Cd_xTe$, the $R(\text{Cd—Te})$ and $R(\text{Hg—Te})$ bond lengths are found to be unchanged relative to the constituents to within 0.001 Å, again in agreement with experiment.[43] In all cases we find that the alloy environment acts to *reduce* the bond-length mismatch, i.e., the bond that is longer in the binary becomes shorter in the alloy, while the shorter of the two binary bonds becomes longer in the alloy. We find that the bond lengths calculated from the SQS-4 model are in good agreement with those calculated from a direct cluster expansion[30] [$R(\text{Zn—Te})=2.656$ Å and $R(\text{Cd—Te})=2.798$ Å for $Cd_{0.5}Zn_{0.5}Te$ and $R(\text{Zn—Te})=2.657$ Å and $R(\text{Hg—Te})=2.789$ Å for $Hg_{0.5}Zn_{0.5}Te$], indicating good convergence of the SQS-4 for bond lengths.

B. Formation enthalpies

The formation enthalpy is defined as the fully optimized total energy of the alloy, measured with respect to the energy of equivalent amounts of the binary constituents at their respective equilibrium structures

$$\Delta H(x)=E(A_{1-x}B_xC)-(1-x)E_{AC}-xE_{BC} . \qquad (12)$$

Using SQS-4 as a model for the random alloy we find at $x=\frac{1}{2}$

$$\Delta H_R =56 \text{ meV}/\text{4-atoms} \quad (Cd_{0.5}Zn_{0.5}Te) ,$$

$$\Delta H_R =49 \text{ meV}/\text{4-atoms} \quad (Hg_{0.5}Zn_{0.5}Te) , \qquad (13)$$

$$\Delta H_R = 10 \text{ meV}/\text{4-atoms} \quad (Hg_{0.5}Cd_{0.5}Te) ,$$

which compare reasonably well with the indirectly determined experimental values[44] ($\pm 100\%$ uncertain) of

$$\Delta H_R =29 \text{ meV}/\text{4-atoms} \quad (Cd_{0.5}Zn_{0.5}Te)$$

$$\Delta H_R =65 \text{ meV}/\text{4-atoms} \quad (Hg_{0.5}Zn_{0.5}Te) \qquad (14)$$

$$\Delta H_R = 16\text{–}30 \text{ meV}/\text{4-atoms} \quad (Hg_{0.5}Cd_{0.5}Te) .$$

[These values of 29, 65, 16, and 30 meV/4-atoms are obtained from Refs. 44(a), 44(a), 44(b), and 44(a), respectively.] Note that $Hg_{0.5}Zn_{0.5}Te$ and $Cd_{0.5}Zn_{0.5}Te$ are considerably less stable thermodynamically (i.e., have larger ΔH) than $Hg_{0.5}Cd_{0.5}Te$ because of the smaller lattice mismatch in the latter alloy. The importance of structur-

TABLE III. Relaxed cell-internal structural parameters of $Cd_{0.5}Zn_{0.5}Te$ and $Hg_{0.5}Zn_{0.5}Te$ in the SQS-4 structure [Eq. (5)]. The unrelaxed structural parameters are given in Eq. (6).

Sublattice	$Cd_{0.5}Zn_{0.5}Te$ $a=6.263$ Å		$Hg_{0.5}Zn_{0.5}Te$ $a=6.269$ Å	
i	x_i	z_i	x_i	z_i
1 Zn	-0.11668	0.0	-0.11633	0.0
2 Cd or Hg	0.36775	0.00339	0.36745	0.00339
3 Te	0.11262	0.26763	0.11206	0.26838
4 Te	-0.36233	0.23403	-0.36181	0.23331

al relaxation, omitted in the VCA and the CPA can be seen by comparing the relaxed values in Eq. (13) to the unrelaxed SQS-4 values ΔH_R^0 calculated at the same molar volume, i.e.,

$$\Delta H_R^0 = 189 \text{ meV}/4\text{-atoms} \quad (\text{Cd}_{0.5}\text{Zn}_{0.5}\text{Te}) ,$$
$$\Delta H_R^0 = 213 \text{ meV}/4\text{-atoms} \quad (\text{Hg}_{0.5}\text{Zn}_{0.5}\text{Te}) . \tag{15}$$

C. Band gaps

We have calculated the direct band gaps at Γ for the equimolar alloys in the SQS-4 model as well as the corresponding band gaps in the binary constituents. The optical bowing coefficient [Eq. (1)] is given at $x = \frac{1}{2}$ as four times the (crystal field averaged) difference between the average band gap of the binary constituents and the calculated band gap of the SQS alloy. Our calculated values are

$$b(\text{Cd}_{0.5}\text{Zn}_{0.5}\text{Te}) = 0.35 \text{ eV} ,$$
$$b(\text{Hg}_{0.5}\text{Zn}_{0.5}\text{Te}) = 0.23 \text{ eV} , \tag{16}$$
$$b(\text{Hg}_{0.5}\text{Cd}_{0.5}\text{Te}) = -0.02 \text{ eV} .$$

These compare reasonably well with the observed low-temperature values of ~ 0.23 eV,[45] ~ 0.14 eV,[46] and 0–0.23 eV,[3,47] for $\text{Cd}_{0.5}\text{Zn}_{0.5}\text{Te}$, $\text{Hg}_{0.5}\text{Zn}_{0.5}\text{Te}$, and $\text{Hg}_{0.5}\text{Cd}_{0.5}\text{Te}$, respectively. Our results differ, however, from previous CPA calculations, e.g., for $\text{Hg}_{1-x}\text{Cd}_x\text{Te}$ Hass et al.[48] obtain ~ 0.27 eV, and Berding et al.[49] find 0.36 eV. For HgZnTe Berding et al.[49] obtained $b = 0.79$ eV. (This calculation corresponds to $T = 0$ K and should hence be compared with low temperature measured values that give[46] $b \sim 0.14$–0.15 eV. The experimental value at room temperature[46] is, however, larger.) Part of the reason for the larger bowing parameters in these CPA calculations[48,49] is that they neglect the metal d bands;[50] since there is a smaller p-d repulsion in the alloy relative to its constituents,[50] the inclusion of an explicit d band reduces bowing relative to calculations that omit d bands. In addition, these CPA calculations [Berding (private communication)] are sensitive to the tight-binding parameters used, in that different tight-binding fits to the band structures of the binaries could yield different bowing parameters in the alloy.

We noticed that for these *common-anion* II-VI systems, the structural relaxation contribution to the band gap $\Delta E = E_g(\text{relaxed}) - E_g(\text{unrelaxed})$ is small and positive: 0.02 and 0.04 eV for $\text{Cd}_{0.5}\text{Zn}_{0.5}\text{Te}$ and $\text{Hg}_{0.5}\text{Zn}_{0.5}\text{Te}$, respectively. This is in contrast with the situation found previously[51(a)] in most *common-cation* semiconductor alloys, where structural relaxation was found to have a larger effect, tending to *reduce* the band gap (i.e., to increase the bowing parameter). The reason for this can be appreciated as follows. When a pair of VCA states at wave vectors $\mathbf{k}_1$ and $\mathbf{k}_2$ fold into the Γ point of the Brillouin zone of a superstructure, creating there states of the same symmetry, they repel each other by the energy proportional to $\Delta V^2/[\epsilon_i(\mathbf{k}_1) - \epsilon_j(\mathbf{k}_2)]$, where ΔV is the difference between the actual and the VCA potential.

For direct band-gap semiconductors this repulsion reduces the band gap. Notice that ΔV has a component arising from the *chemical* differences (between VCA and the actual A-type and B-type potentials) and another component due to structural relaxation. We found previously[51(a)] that structural relaxation enhances the perturbing potential ΔV, hence increases the level repulsion, reducing thereby the band gap. Furthermore, this level repulsion exists both in the valence band and in the conduction band in common-cation alloys.[51(a)] In contrast, in II-VI common-anion systems this level repulsion exists primarily in the conduction bands; there the energy denominator is considerably larger than in III-V systems, hence the repulsion and band-gap reduction are smaller. In the II-VI alloys, an additional mechanism is at play: in $\text{Cd}_{0.5}\text{Zn}_{0.5}\text{Te}$ both the valence-band maximum (VBM) and the conduction band minimum (CBM) have more Zn than Cd character.[20] Since the structural relaxation reduces the Zn—Te bond length, this *increases* the band gap slightly by lowering the energy of the bonding VBM and raising the energy of the antibonding CBM. This overwhelms the level repulsion effect, leading to a small *increase* (0.02 eV) in the alloy's band gap upon relaxation. In $\text{Hg}_{0.5}\text{Zn}_{0.5}\text{Te}$, on the other hand, both the CBM and the VBM have more Hg than Zn character.[20] Structural relaxation, leading to a *longer* Hg—Te bond *reduces* the band gap. However, the VBM is repelled also upwards by the lower lying d states.[20] Since longer Hg—Te bonds diminish this repulsion, this moves the VBM to lower energies, raising the band gap. The net effect is that structural relaxation raises slightly (by 0.04 eV) the band gap.

Since the situation for the Zn-Cd-Te systems is quite typical of most *common-anion* isovalent semiconductor alloys, the arguments above suggest that structural relaxation effects on the optical bowing are rather small in these systems: they are either slightly positive (for most III-V systems[51(b)]) or slightly negative (for most II-VI systems). For *common-cation* systems on the other hand, the atomic p energy levels decrease with atomic size in a given column of the Periodic Table (e.g., the calculated semirelativistic LDA eigenvalues for S, Se, and Te valence p levels are -7.19, -6.74, and -6.19 eV, respectively), hence both level repulsion and level shift act to reduce the band gap. In this case, structural relaxation is significant.[32,51]

VI. ALLOY DENSITY OF STATES

A. Models considered

Figures 6–8 depict the calculated densities of states of the three alloy systems studied. For each we compare the following three results.

(i) First is the DOS of a "quasi-VCA" (QVCA) alloy model obtained from the concentration-weighted eigenvalues of the constituents

$$\bar{\epsilon}_j(\mathbf{k}) = \frac{1}{2}[\epsilon_j^{AC}(\mathbf{k}) + \epsilon_j^{BC}(\mathbf{k})] , \tag{17}$$

where all energies are calculated at a fixed alloy volume

V. This model considers the influence of volume deformation on the *averaged* constituents, but does not include the chemical effects (i.e., charge transfer) or positional relaxation. Like the VCA, this approximation results in an identical number of DOS peaks in the alloy and its constituents.

(ii) Second is the DOS of the *unrelaxed* SQS-N [using the parameters of Eq. (6), hence the same bond lengths as in the QVCA model]. Since, however, atoms are not averaged in this SQS model, comparison with the QVCA results reflects the effects of the (constant-volume) *chemical perturbation*. Previous studies[40] indicated that the S-CPA mimics the results of this model for lattice-matched $Al_{1-x}Ga_xAs$ if weak to medium chemical perturbation is assumed in a tight-binding model.

(iii) Third is the DOS of the *relaxed* SQS-N (using the parameters of Table III). Comparison with the DOS of the unrelaxed structure provides a measure of *structural relaxation* effects on the DOS.

B. The lattice-matched alloy $Hg_{0.5}Cd_{0.5}Te$

Figure 6 depicts the DOS of $Hg_{0.5}Cd_{0.5}Te$; because of the close lattice match between the constituents, relaxation effects are negligible, and have been neglected here. The difference between the QVCA and the SQS calculations hence reflects the changes due to chemical disorder alone. Chemical disorder is seen to be weak in the $P1$ and $P4$ regions: these states exhibit only alloy broadening (relative to the corresponding QVCA states), but no significant splitting. The largest chemical disorder effect is evident in the $P2$ region which corresponds to the metal-centered localized d states (Table II). The spin-orbit doublets ($j = \frac{3}{2}$ and $\frac{5}{2}$) of CdTe and HgTe appear in the alloy [Figs. 6(c)–6(d)] in the sequence $Cd\frac{3}{2} < Cd\frac{5}{2} < Hg\frac{3}{2} < Hg\frac{5}{2}$, consistent with photoemission measurements.[52] Note that upon alloying, the Cd $4d$ moves to a deeper binding energy (relative to the VBM), while the Hg $5d$ is displaced to a lower binding energy, as observed experimentally.[52] The reason for this shift is that the VBM of HgTe is higher in absolute energy (by ~ 0.35 eV) (Refs. 20 and 52) than the VBM of CdTe.

The most interesting spectral regions in this material are the sp^3 bonding $P3$ bands and antibonding $P5$ bands which have large cation s character (Table II). Since in the zinc-blende compounds the Hg $6s$ states have considerably deeper binding energies than the Cd $5s$ states [compare the energies of $P3$ and $P5$ in the two binaries in Figs. 6(a) and 6(e)], these states split in the alloy. The DOS shows distinct peaks [Figs. 6(c) and 6(d) associated with HgTe (with deeper binding energy) and with CdTe (with shallower binding energy). This splitting (~ 0.7 eV) and broadening does not exist in the VCA-type calculation [Fig. 6(b)] which lacks the chemical perturbation potential.

Since the SQS-4 structure contains only the A_3B and AB_3 tetrahedra in the 1:1 ratio, the adequacy of the SQS-4 model is tested by calculating DOS of $Hg_{0.5}Cd_{0.5}Te$ in the more accurate (but time consuming) SQS-8 model. The charge density is converged with four special $\mathbf{k}$ points in the irreducible Brillouin zone of the

SQS-8. We have averaged over the two variants of the SQS-8 (see Sec. V A) which contain all five A_4, A_3B, A_2B_2, AB_3, and B_4 tetrahedra in the random probability ratio 1:4:6:4:1. The results are given in Fig. 6(d). Comparing the DOS in Figs. 6(c) and 6(d) we see that, except for some fine changes in the shape of the DOS, all the basic features (splitting, broadening, etc.) are contained in the SQS-4 model. Hence, in the following discussion, unless necessary, we will use SQS-4 structure to describe the feature of the alloy DOS.

A number of previous DOS calculations exist for $Hg_{1-x}Cd_xTe$. Spicer et al.,[15,53] Shih et al.,[52] and Chen and Sher[54] used a combined empirical pseudopotential and tight-binding Hamiltonian in a four-orbital per atom $(s, 3p)$ Gaussian basis set to perform single-site CPA calculations in the diagonal-disorder approximation. The
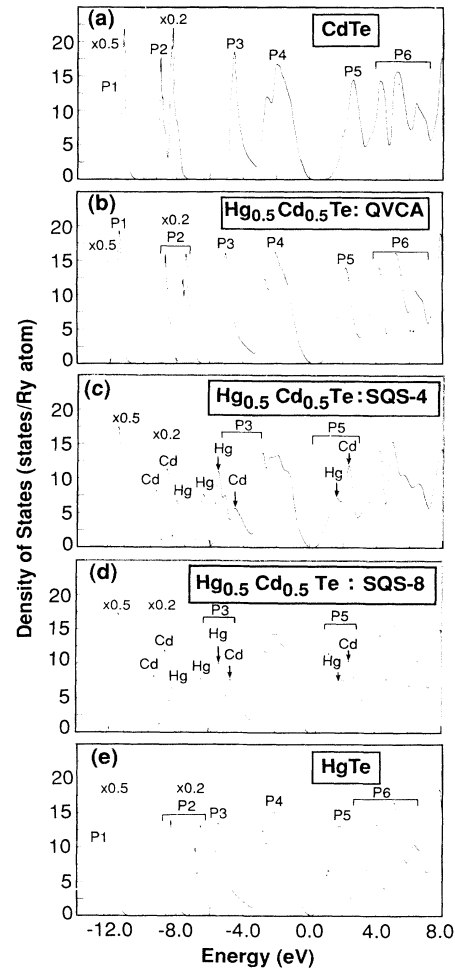
FIG. 6. Total DOS for the HgTe-CdTe system: (a) CdTe, (b) $Hg_{0.5}Cd_{0.5}Te$ in the QVCA model, (c) $Hg_{0.5}Cd_{0.5}Te$ in the SQS-4 model, and (d) $Hg_{0.5}Cd_{0.5}Te$ in the SQS-8 model averaged over its two variants, and (e) HgTe. All the DOS are calculated at the $x = \frac{1}{2}$ alloy lattice constant $a = 6.480$ Å. Notice the change of scale for the $P1$ and $P2$ peaks. Zero of energy is at the VBM.

nine tight-binding parameters were adjusted to fit the band energies of the binary constituents in a number of high-symmetry points in the zone, the CdTe effective mass at Γ_{1c}, and spin-orbit splitting. Self-consistency, CdTe/HgTe band offset as well as cation d bands were neglected. They find that the $P1$ peak is split into two components in HgTe as well as in the alloy treated by the VCA [unlike our result in Figs. 6(e) and 6(b), respectively], while the CPA result shows a single, broader $P1$ peak. (We noticed that,[20] although the splitting in the $P1$ region is common in III-V compounds, the existence of cation d states inside the valence bands in II-VI compounds acts to narrow the $P1$ peak by s-d repulsion. This diminishes the splitting.) The $P2$ region is missing from their spectrum as cation d bands were omitted. In the $P3$ region Spicer et al. find a single, narrow peak in VCA at $x=0.3$, whereas in the S-CPA this broadens and splits into a Hg-like s peak at $E_v - 5.6$ eV, a Cd s shoulder at $E_v - 4.2$ eV, and a hybridized sp structure at $E_v - 5.0$ eV. The occurrence of separate Hg-like and Cd-like features is in agreement with the photoemission data[15,53] and constitutes the first clear example of the breakdown of the VCA in semiconductor alloys. The $P4$, $P5$, and $P6$ regions of the spectrum are only broadened slightly in the CPA relative to the VCA.

Hass et al.[48,55] and Ehrenreich and Hass[56] used an eight-orbital per atom $(2s + 6p)$ next-nearest neighbor empirical tight binding Hamiltonian with spin-orbit splitting (no metal d orbitals) to compute the CPA spectrum of $Hg_{1-x}Cd_xTe$ in the site-diagonal disorder approximation. The $P1$ and $P2$ regions were not shown. The CPA calculation shows broadening of the $P3$ density of states and an increased splitting; it splits at $x=0.30$ into a Hg,s peak at $E_v - 5.2$ eV, and a Cd s shoulder at $E_v - 4.6$ eV; the intermediate sp peak found by Chen and Sher[54] and Spicer et al.[15,53] is missing, and was argued[55] to arise from certain simplifying approximations in the CPA work of Refs. 15, 53, and 54. A similar splitoff behavior was also predicted[48] to occur at $x=0.3$ in the $P5$ region, around $E_v + 3$ eV. The $P4$ and $P5$ regions were similar in the VCA and the CPA.

Kudrovsky et al.[57,58] have recently developed a new, first-principles method for calculating the electronic structure of random alloys, based on the tight-binding representation of the linear muffin-tin orbital (LMTO) method. They consider four interpenetrating fcc sublattices. For $A_{1-x}B_xC$ alloys, one is occupied at random by A or B, the second by C_A or C_B (the C atoms in AC and BC, respectively), and the other two sublattices are occupied by interstitial spheres. To each site they assign the distinct potential parameters corresponding to A, B, C_A, and C_B with appropriate random probabilities. The application to $Hg_{1-x}Cd_xTe$ yielded (i) broadening of $P1$ due to off-diagonal disorder, (ii) splitting of $P2$ into two components (rather than four, since the spin-orbit interaction was omitted) associated with Hg $5d$ and Cd $4d$, (iii) splitting of $P3$ into two components associated with Hg s and Cd s, (iv) weak disorder effects on $P4$, and (v) splitting of $P5$ into two components. All of these features are qualitatively the same as in the present calculation.

C. The lattice-mismatched $Cd_{0.5}Zn_{0.5}Te$ and $Hg_{0.5}Zn_{0.5}Te$ alloys

To our knowledge, there are no previous calculations on the density of states of $Hg_{1-x}Zn_xTe$ and $Cd_{1-x}Zn_xTe$ alloys, except for a preliminary CPA study of the band-gap region in[49] $Hg_{1-x}Zn_xTe$. Figures 7 and 8 depict our results.

(i) The P1 region. In the Te-localized $P1$ regions we observe a split-band behavior, absent in the VCA. This is a clear case where the chemical disorder in the common
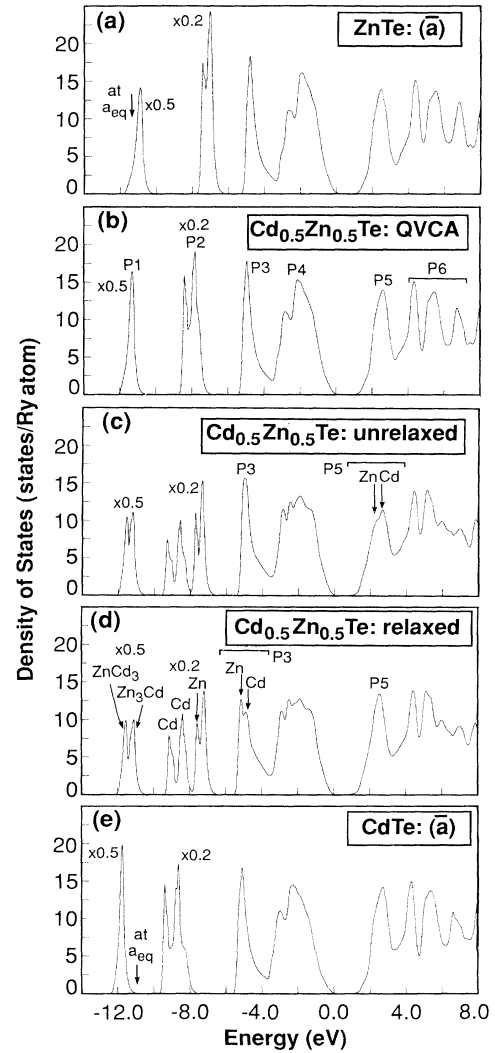
FIG. 7. Total DOS for the ZnTe-CdTe system: (a) ZnTe, (b) $Cd_{0.5}Zn_{0.5}Te$ in the QVCA model, (c) $Cd_{0.5}Zn_{0.5}Te$ in the unrelaxed SQS-4 model, (d) same as (c) but relaxed, and (e) CdTe. All the DOS are calculated at the $x = \frac{1}{2}$ average lattice constant $\bar{a} = 6.263$ Å. Notice the change of scale for the $P1$ and $P2$ peaks. In parts (a) and (e) we indicate by vertical arrows the positions of the $P1$ peaks of the zinc-blende constituents at their respective individual equilibrium volumes. Zero of energy is at the VBM.

sublattice potential produces a splitting, an effect which is qualitatively missing in standard CPA models (where all C atoms are taken to be chemically identical). Although $P1$ has mostly the orbital character of Te,s, different coordinations of Te by $A_{4-n}B_n$ ligands affect its energy. Inspection of the electronic charge densities in the $P1$ region in the alloys [e.g., Figs. 9(c) and 9(d) for $Hg_{0.5}Zn_{0.5}Te$] shows that the split components are associated with different tetrahedral coordination about Te (a "ligand-field" effect). For $Cd_{0.5}Zn_{0.5}Te$ in the SQS-4 structure [Fig. 7(d)], the deeper of the two $P1$ peaks is

due to Te-centered $ZnCd_3$ tetrahedron while the shallower peak is due to a Zn_3Cd tetrahedral coordination. For $Hg_{0.5}Zn_{0.5}Te$ in the SQS-4 structure [Fig. 8(d)] the deeper of the two $P1$ peaks ["high binding energy $P1$" in Fig. 9(d)] is due to $ZnHg_3$, whereas the shallower peak [Fig. 9(c)] is due to the Zn_3Hg tetrahedron. The reason for this sequence of states can be appreciated as follows. As indicated in Table I, the partial molar volumes of ZnTe (CdTe or HgTe) are dilated (compressed) in the alloy. Consequently, their atom-centered states move in the alloy to shallower (deeper) binding energies relative to the VBM [see Figs. 7 and 8 in which the vertical arrows in parts (a) and (e) show the position of $P1$ in the binaries at their respective equilibrium volume]. The splitting observed in the $P1$ regions of the alloy correspond to a superposition of these *volume-shifted* states, modified slightly by the alloy interactions. Note that in the absence of a volume deformation, the two $P1$ doublets in $Cd_{0.5}Zn_{0.5}Te$ would be nearly degenerate, in opposition to what we find in the (volume-relaxed) calculations. Structural disorder
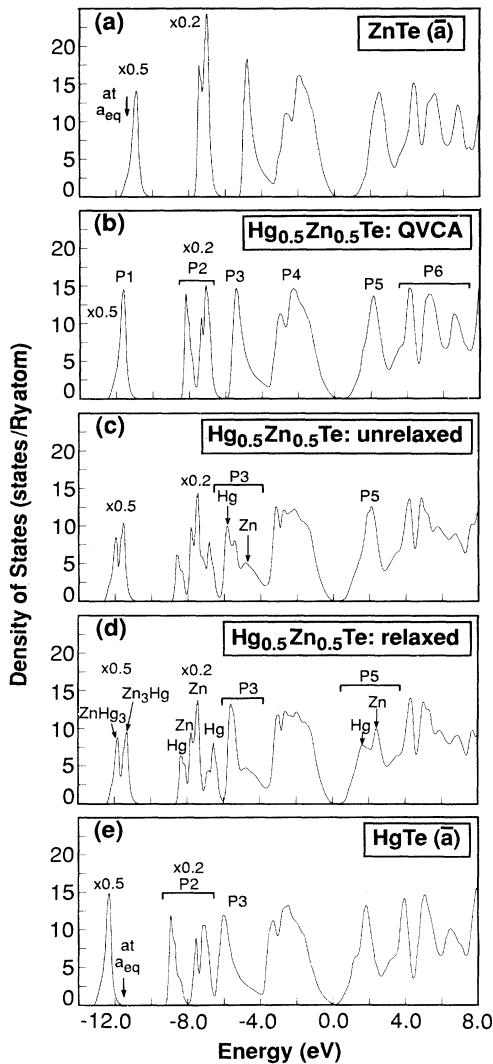
FIG. 8. Total DOS of the ZnTe-HgTe system: (a) ZnTe, (b) $Hg_{0.5}Zn_{0.5}Te$ in the QVCA model, (c) $Hg_{0.5}Zn_{0.5}Te$ in the unrelaxed SQS-4 model, (d) same as (c) but relaxed, and (e) HgTe. All the DOS are calculated at the $x = \frac{1}{2}$ average lattice constant $\bar{a}=6.269$ Å. Notice the change of scale for the $P1$ and $P2$ peaks. In parts (a) and (e) we indicate by vertical arrows the positions of the $P1$ peaks of the zinc-blende constituents at their respective *individual* equilibrium volumes. Zero of energy is at the VBM.
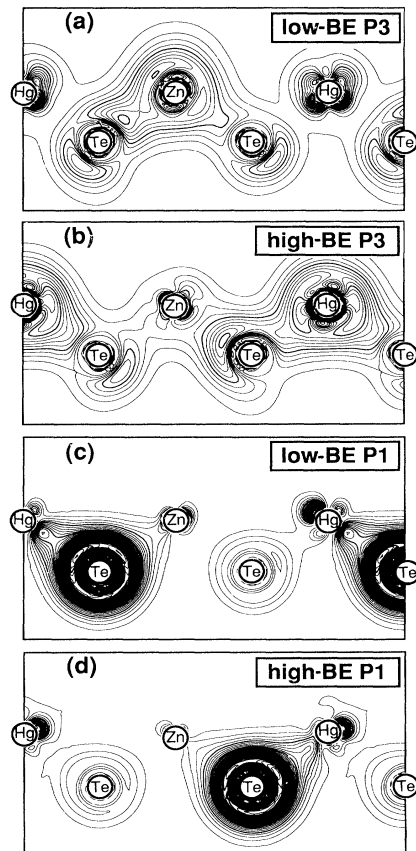
FIG. 9. Charge-density contour plot for $Hg_{0.5}Zn_{0.5}Te$ in the energy ranges (a) $P3$ showing the lower binding energy Zn-localized peak, (b) $P3$ showing the higher binding energy Hg-localized peak, (c) $P1$ showing the lower binding energy peak, and (d) $P1$ showing the higher binding energy peak [see Fig. 8(d)]. Each peak is normalized to contain $2e$ per zinc-blende cell. The contour step size is 2×10^{-3} $e/a.u.^3$.

effects are rather small in the $P1$ region: since the $P1$ states have atom-centered wave functions, they respond mostly to volume changes rather than to bond-length deformations. Indeed, the $P1$ region is relatively unchanged in going from unrelaxed [Figs. 7(c) and 8(c)] to the relaxed [Figs. 7(d) and 8(d)] geometries. We noticed that the existence of only two peaks in the $P1$ region is an artifact of our using the SQS-4 model which contains only two types (A_3B and AB_3) tetrahedra. As one progresses from the SQS-4 structure to the SQS-8 structure (averaged over the two variants) which contains all five (A_4, A_3B, A_2B_2, AB_3, and B_4) type tetrahedra in the random probability ratio, one expects to find further splittings and broadening in this region. Figure 10 shows the calculated DOS of $Cd_{0.5}Zn_{0.5}Te$ in the unrelaxed, 16-atom SQS-8 structure; in this figure we have also included the DOS without Gaussian broadening [Fig. 10(b)] so that fine details can be seen. We see that the $P1$ peak exhibits fine structure on the scale of ~ 0.2 eV; an analysis of these structures shows that they represent the signatures of the five $A_{4-n}B_n$ ($0 \leq n \leq 4$) tetrahedra with random possibilities. If a broadening of 0.2 eV is used [Fig. 10(a)], these features are washed out. In principle, therefore, an "ideal" high-resolution photoemission experiment should observe the signature of *all* clusters [Fig. 10(b)]. Conventional S-CPA produces a single $P1$ peak at *all* resolutions.

(ii) *The P2 region.* The cation d orbital $P2$ regions exhibit a similar "superposition of states" as observed in $Hg_{0.5}Cd_{0.5}Te$. Again, structural relaxation plays a minor role here except for the Hg $5d$ states in $Hg_{0.5}Zn_{0.5}Te$, which exhibit significant pd bonding in this region:[20]
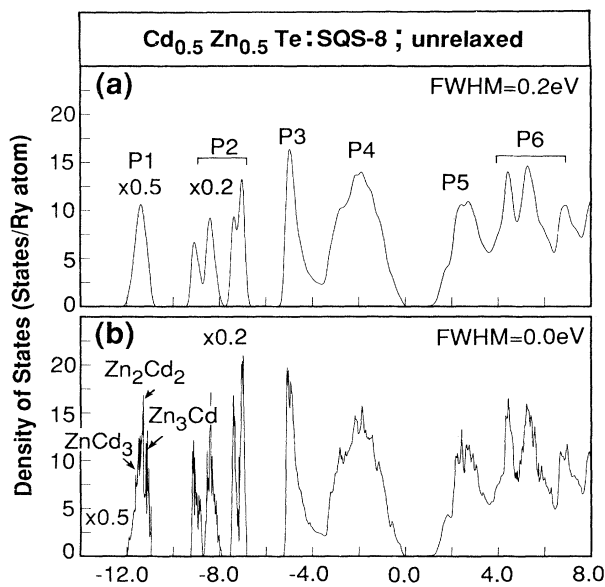
FIG. 10. Total DOS for the ZnTe-CdTe system calculated using the unrelaxed SQS-8 structures with $\bar{a} = 6.263$ Å, (a) with Gaussian broadening and FWHM $= 0.2$ eV and (b) no broadening. The results are averaged over the two variants of the SQS-8 structures. Notice the change of scale for the $P1$ and $P2$ peaks.

upon relaxation, the Hg—Te bond is elongated (Fig. 1), hence $P2$ moves towards the VBM. We find that the order of the spin-orbit splitting states are nested differently: for $Cd_{0.5}Zn_{0.5}Te$ it is $Cd\frac{3}{2} < Cd\frac{5}{2} < Zn\frac{3}{2} < Zn\frac{5}{2}$, whereas in $Hg_{0.5}Zn_{0.5}Te$ it is $Hg\frac{3}{2} < Zn\frac{3}{2} < Zn\frac{5}{2} < Hg\frac{5}{2}$. These results are consistent with the calculated[20] sequence of the spin-orbit splittings $\Delta_d(ZnTe) = 0.37$, $\Delta_d(CdTe) = 0.69$, and $\Delta_d(HgTe) = 1.70$ eV and d-band centers in the *zinc-blende constituents*, reported previously.[20,59] However, in $Hg_{1-x}Zn_xTe$ the metal d states observed experimentally[8(c),52] have a different order,

$$Zn\frac{3}{2} < Zn\frac{5}{2} \approx Hg\frac{3}{2} < Hg\frac{5}{2} . \tag{18}$$

The reason for this discrepancy is that the LDA error in the calculated d-band centers increases with the localization of the states: Since the Zn $3d$ wave functions are more localized than the Cd $4d$ wave functions, and the latter are more localized than Hg $5d$, the LDA errors (~ 2.7, 2.2, and 1.4 eV for the d-band centers in ZnTe, CdTe, and HgTe, respectively[20]) decrease in the same order.

We find that the binding energies (relative to the VBM) of the metal d states in $Hg_{0.5}Zn_{0.5}Te$ are similar to those in binaries *at equilibrium* (Fig. 2), reflecting a smaller natural valence band offset in this system.[20,52] No shift was observed in the metal d binding energy in $Hg_{0.84}Zn_{0.16}Te$ alloys.[52] Small changes (< 0.17 eV) were observed in Ref. 29 for $Hg_{1-x}Zn_xTe$. These are consistent with the present calculations.

(iii) *The P3 and P5 regions.* In the sp^3 bonding $P3$ and antibonding $P5$ regions we observe qualitatively similar chemical disorder effects as seen in $Hg_{0.5}Cd_{0.5}Te$: the single VCA $P3$ peaks splits in $Cd_{0.5}Zn_{0.5}Te$ into [Figs. 7(c) and 7(d)] a Zn,s state and a Cd,s state while in $Hg_{0.5}Zn_{0.5}Te$ [Figs. 8(c) and 8(d)] it splits into Hg,s and Zn,s. The wave-function amplitudes for $Hg_{0.5}Zn_{0.5}Te$ in this $P3$ region are shown in Figs. 9(a) and 9(b). For unrelaxed structures these splittings are -0.1 eV in $Cd_{0.5}Zn_{0.5}Te$ and 0.5 eV in $Hg_{0.5}Zn_{0.5}Te$ (positive values indicate that the heavier atom has a higher binding energy). However, in contrast with $Hg_{0.5}Cd_{0.5}Te$, we observe here for the lattice-mismatched alloys a strong *structural relaxation* effect: in $Cd_{0.5}Zn_{0.5}Te$, the $P3$ splitting is *induced* by relaxation while the $P5$ splitting is *eliminated* by relaxation [compare Figs. 7(c) and 7(d)]. Conversely, in $Hg_{0.5}Zn_{0.5}Te$, the $P3$ splitting is *eliminated* by relaxation while the $P5$ splitting is *induced* by relaxation [compare Figs. 8(c) and 8(d)]. This is a clear manifestation of (nonhydrostatic) structural relaxation effects absent in the conventional S-CPA models.

To understand the changes of the DOS associated with lattice relaxation we have plotted semiquantitatively in Fig. 11 the sp^3 bonding and antibonding energy levels for the unrelaxed (equal bond length) $Cd_{0.5}Zn_{0.5}Te$ and $Hg_{0.5}Zn_{0.5}Te$ alloys. Note that for isovalent cations the atomic valence p energy levels are very similar (using semirelativistic LDA we find -1.31, -1.41, and -1.26 eV for Zn $4p$, Cd $5p$, and Hg $6p$ states, respectively), while the valence s energy levels exhibit a significant variation (we find -6.31, -6.04, and -7.21 eV for Zn $4s$, Cd
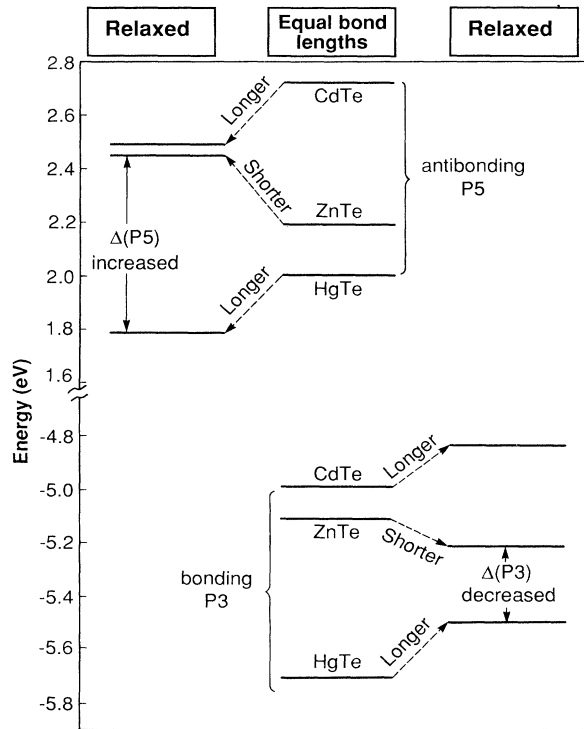
FIG. 11. Calculated relaxation-induced energy-level shifts in the peak of the projected sp^3 bonding and antibonding states for $Cd_{0.5}Zn_{0.5}Te$ and $Hg_{0.5}Zn_{0.5}Te$ systems. For convenience we have aligned the ZnTe states of the two unrelaxed systems. "Longer" and "shorter" refer to changes in bond lengths (relative to the VCA average) upon relaxation; see Fig. 1 and Table I.

5s, and Hg 6s states, respectively; the lower s orbital energy for Hg is due to its large relativistic s shift). Hence, for a fixed (unrelaxed) cation—anion bond length, the trends in the sp^3 bonding and antibonding energy levels are dominated by the order of the cation s orbital energies, e.g.,

$$\epsilon(HgTe, sp^3) < \epsilon(ZnTe, sp^3) < \epsilon(CdTe, sp^3) , \qquad (19)$$

depicted in the central panel of Fig. 11. Relaxation shifts these energy levels: since P3 and P5 are bond-centered and antibond centered states, respectively, they respond through their deformation potentials primarily to changes in *bond lengths*. To see how these relaxations affect the energies of P3 and P5 note first from Table I and Fig. 1 that upon relaxation of $Cd_{0.5}Zn_{0.5}Te$ and $Hg_{0.5}Zn_{0.5}Te$, the Zn—Te bond becomes *shorter* while the Cd—Te or Hg—Te bonds becomes *longer* relative to the average VCA values (these trends are indicated in Fig. 11 by the words "longer" and "shorter"). Second, note that in zinc-blende semiconductors the deformation potentials are such that the bonding states (P3) move to larger (deeper) binding energies when the bonds are shortened, while antibonding states (P5) move to lower binding energies.[60] Conversely, when bonds are elongated, bonding (antibonding) states move to smaller (larger) binding energies. These changes are indicated in Fig. 11 by the direc-

tions of the arrows. Our LAPW calculated relaxation-induced shifts in the bonding and antibonding energies are depicted in Fig. 11. We see that they agree with the qualitative trends expected above. The net effect of structural relaxation is, therefore, to (a) *reduce* the energy-level separation $\Delta(P5)$ between antibonding (P5) CdTe-like and ZnTe-like states in $Cd_{0.5}Zn_{0.5}Te$, but *increase* the level separation $\Delta(P3)$ for the corresponding bonding P3 states; (b) *increase* the energy-level separation $\Delta(P5)$ between antibonding (P5) ZnTe-like and HgTe-like states in $Hg_{0.5}Zn_{0.5}Te$, but *reduce* the separation $\Delta(P3)$ between the corresponding bonding (P3) states. These trends are evident in our calculated DOS shown in Figs. 7(c), 7(d), 8(c) and 8(d). We see that the different responses of the density of states of $Cd_{0.5}Zn_{0.5}Te$ and $Hg_{0.5}Zn_{0.5}Te$ in the P3 and P5 regions to relaxation reflect the fact that Hg has a deeper s valence orbital energy relative to Zn, but that Cd has a shallower s orbital energy relative to Zn. The situation in $Cd_{0.5}Zn_{0.5}Te$ is similar to that in $In_{0.5}Ga_{0.5}As$: using the molecular CPA, Hass *et al.*[32] found qualitatively similar effects in the latter. These effects are missed by conventional S-CPA approach.

(iv) *The P4 and P6 regions.* The complementary P4 and P6 regions in the DOS represent rather extended states which show broadening relative to the QVCA and little structural relaxation effects. The scattering is generally weak in these regions since they are mostly anion and cation p states, for which the atomic orbital energy differences are small.[20]

VII. SUMMARY

We have calculated the electronic structure of the random II-VI telluride semiconductor alloys $Cd_{0.5}Zn_{0.5}Te$, $Hg_{0.5}Zn_{0.5}Te$, and $Hg_{0.5}Cd_{0.5}Te$, studying both chemical and structural disorder effects using the new special quasirandom structures approach. We find the following.

(i) Chemical disorder is responsible for most of the broadening and splitting of the atom-centered and volume-extended features in the DOS. For the three II-VI systems studied here we find that this chemical disorder induces significant splittings at the bottom of the valence bands (P1), at the metal d states (P2), the bottom of the upper valence bands (P3), and at the top of the first conduction bands (P5). These observations are consistent with available experimental data but not with the VCA.

(ii) The splitting caused by the structural relaxation is as important as chemical disorder effects for bond-localized and antibond-localized states, e.g., the sp^3 bonding states (P3) at the bottom of the upper valence bands and the sp^3 antibonding states (P5) in the first conduction bands. We found that this effect causes a reverse splitting in ZnCdTe versus ZnHgTe, and explained this in terms of a simple tight-binding model.

(iii) Structural relaxation effects on optical bowing of the fundamental band gap are found to be smaller for common-anion systems than for common-cation systems.

Compared to the molecular CPA, the SQS approach

has the advantage of treating all relaxation effects on equal footing and permitting effective use of first-principles electronic-structure methods. The accuracy of the SQS approach can be systematically improved by increasing the size of the unit cell. While we prefer the SQS-8 model, many of the basic features are already contained in the SQS-4 model. On the other hand, in this approach one has to use different SQS's at different compositions x. When x is close to 0 (or 1), large SQS's have to be used. In this respect, the molecular CPA can treat more efficiently trends in alloy properties with composition, as long as an accurate Hamiltonian is used.

ACKNOWLEDGMENTS

[1] J. C. Woolley, in *Compound Semiconductors*, edited by R. K. Willardson and H. L. Goering (Reinhold, New York, 1962), p. 3.

[2] N. K. Abrikosov, V. F. Bankina, L. V. Poretskaya, L. E. Shelimova, and E. V. Skudnova, *Semiconducting II-VI, IV-V, and V-VI Compounds* (Plenum, New York, 1969).

[3] *Numerical Data and Functional Relationships in Science and Technology*, Vol. 17a,b of *Landolt-Börnstein New Series*, edited by O. Madelung, M. Schulz, and H. Weiss (Springer-Verlag, Berlin, 1982).

[4] L. Vegard, Z. Phys. **5**, 17 (1921).

[5] J. E. Jaffe and A. Zunger, Phys. Rev. B **28**, 5822 (1983).

[6] L. Nordheim, Ann. Phys. (Leipzig) **9**, 607 (1931).

[7] P. Soven, Phys. Rev. **156**, 809 (1967); B. Velický, S. Kirkpatrick, and H. Ehrenreich, *ibid.* **175**, 747 (1968).

[8] (a) J. C. Mikkelsen and J. B. Boyce, Phys. Rev. Lett. **49**, 1412 (1982); Phys. Rev. B **28**, 7130 (1983); (b) N. Motta, A. Balzarotti, P. Letardi, A. Kisiel, M. T. Czyzyk, M. Zimnal-Starnawska, and M. Podgorny, Solid State Commun. **53**, 509 (1985); (c) A. Marbeuf, D. Ballutaud, R. Triboulet, H. Dexpert, P. Lagarde, and Y. Marfaing J. Phys. Chem. Solids **50**, 975 (1989).

[9] A. N. Pikhtin, Fiz. Tekh. Poluprovodn. **11**, 425 (1977) [Sov. Phys.—Semicond. **11**, 245 (1977)]; D. Z. Y. Ting and Y. C. Chang, Phys. Rev. B **30**, 3309 (1984). If one denotes as $\Psi_i(\mathbf{k})$ and $\Psi_f(\mathbf{k}')$ ($\mathbf{k} \neq \mathbf{k}'$ in the zinc-blende Brillouin zone) the initial- and final-state wave functions of certain configurations, respectively, and by $\langle \ \rangle$ a configuration average in the random alloy, the dipole (**P**) transition probability $\int \langle \Psi_i \rangle \mathbf{P} \langle \Psi_f \rangle d\mathbf{r} = 0$ vanishes (since $\langle \Psi_i \rangle$ and $\langle \Psi_f \rangle$ have their respective zinc-blende symmetry), while the correct result $\langle \int \Psi_i \mathbf{P} \Psi_f d\mathbf{r} \rangle \neq 0$ can be finite.

[10] R. Weil, R. Nkum, E. Muranevich, and L. Benguigui, Phys. Rev. Lett. **62**, 2744 (1989).

[11] K. Beshah, D. Zamir, P. Becla, P. A. Wolff, and R. G. Griffin, Phys. Rev. B **36**, 6420 (1987).

[12] D. E. Zax, S. Vega, N. Yellin, and D. Zamir, Chem. Phys. Lett. **130**, 105 (1987).

[13] A. Kobayashi and A. Roy, Phys. Rev. B **35**, 5611 (1987).

[14] R. Carles, G. Landa, and J. B. Renucci, Solid State Commun. **53**, 179 (1985).

[15] W. E. Spicer, J. A. Silberman, J. Morgan, I. Lindau, J. A. Wilson, A.-B. Chen, and A. Sher, Phys. Rev. Lett. **49**, 948 (1982).

[16] K. L. Tsang, J. E. Rowe, T. A. Callcott, and R. A. Logan, Phys. Rev. B **38**, 13 277 (1988).

[17] See recent review articles in *Local Density Approximations in Quantum Chemistry and Solid State Physics*, edited by J. P. Dahl and J. Avery (Plenum, New York, 1982).

[18] S.-H. Wei and H. Krakauer, Phys. Rev. Lett. **55**, 1200 (1985).

[19] L. Hedin and B. I. Lundqvist, J. Phys. C **4**, 2063 (1971).

[20] S.-H. Wei and A. Zunger, Phys. Rev. B **37**, 8958 (1988).

[21] D. J. Chadi and M. L. Cohen, Phys. Rev. B **8**, 5747 (1973).

[22] G. Lehmann and M. Taut, Phys. Status Solidi **54**, 469 (1971).

[23] A. H. MacDonald, W. E. Pickett, and D. Koelling, J. Phys. C **13**, 2675 (1980); W. E. Pickett, A. J. Freeman, and D. D. Koelling, Phys. Rev. B **23**, 1266 (1981).

[24] e.g., see J. P. Perdew and A. Zunger, Phys. Rev. B **23**, 5048 (1981).

[25] L. Ley, R. A. Pollak, F. R. McFeely, S. P. Kowalczyk, and D. A. Shirley, Phys. Rev. B **9**, 600 (1974); N. J. Shevchik, J. Tejeda, and M. Cardona, *ibid.* **9**, 2627 (1974); N. J. Shevchik, J. Tejeda, M. Cardona, and D. W. Langer, Phys. Status Solidi B **59**, 87 (1973).

[26] A. Zunger, Phys. Rev. Lett. **50**, 1215 (1983).

[27] L. J. Sham and M. Schluter, Phys. Rev. Lett. **51**, 1888 (1983).

[28] J. P. Perdew and M. Levy, Phys. Rev. Lett. **51**, 1884 (1983).

[29] G. Martinez, in *Handbook on Semiconductors*, edited by M. Balkanski (North-Holland, Amsterdam, 1980), Vol. 2, p. 181.

[30] S.-H. Wei, L. G. Ferreira, and A. Zunger, Phys. Rev. B **41**, 8240 (1990).

[31] A.-B. Chen, and A. Sher, Phys. Rev. B **17**, 4726 (1978); A. Bieber and F. Gautier, Physica B **107**, 71 (1981).

[32] K. C. Hass, R. Lempert, and H. Ehrenreich, Phys. Rev. Lett. **52**, 77 (1984); R. Lempert, K. C. Hass, and H. Ehrenreich, Phys. Rev. B **36**, 1111 (1987).

[33] R. Mills and P. Ratanavararaka, Phys. Rev. B **18**, 5291 (1978); T. Kaplan, P. L. Leath, L. J. Gray, and H. W. Diehl, *ibid.* **21**, 4230 (1980).

[34] A. Zin and E. A. Stern, Phys. Rev. B **31**, 4954 (1985); E. A. Stern and A. Zin, *ibid.* **9**, 1170 (1974).

[35] L. C. Davis and H. Holloway, Solid State Commun. **64**, 121 (1987); L. C. Davis, Phys. Rev. B **28**, 6961 (1983).

[36] R. Alben, M. Blume, H. Krakauer, and L. Schwartz, Phys. Rev. B **12**, 4090 (1975); R. Alben, M. Blume, and M. McKewon, *ibid.* **16**, 3829 (1977).

[37] S. Lee, D. M. Bylander, and L. Kleinman, Phys. Rev. B **40**, 8399 (1989).

[38] A. Zunger, S.-H. Wei, L. G. Ferreira, and J. E. Bernard, Phys. Rev. Lett. **65**, 353 (1990).

[39] (a) S.-H. Wei, L. G. Ferreira, J. E. Bernard, and A. Zunger, Phys. Rev. B **42**, 9622 (1990); (b) S.-H. Wei and A. Zunger, Appl. Phys. Lett. **56**, 662 (19990); (c) J. E. Bernard and A. Zunger (unpublished).

[40] K. Hass, L. C. Davis, and A. Zunger, Phys. Rev. B **42**, 3757

(1990).

[41]P. N. Keating, Phys. Rev. **145**, 637 (1966).

[42]J. L. Martins and A. Zunger, Phys. Rev. B **30**, 6217 (1987).

[43]A. Balzarotti, Physica B **146**, 150 (1987).

[44](a) A. Laugies, Rev. Phys. Appl. **8**, 259 (1973); (b) C. H. Su, P. K. Liao, and R. F. Brebrick, J. Electrochem. Soc. **132**, 942 (1985). Value taken at $T=1000$ K.

[45]V. G. Sredin, Fiz. Tekh. Poluprovodn. **12**, 1830 (1978) [Sov. Phys.—Semicond. **12**, 1084 (1978)].

[46](a) B. Toulouse, R. Granger, S. Roll, and R. Triboulet, J. Phys. (Paris) **48**, 247 (1987), find for Hg-Zn-Te $b=0.14$ eV; (b) A. Sher, D. Eger, A. Zemel, H. Feldstein, and A. Raizman, J. Vac. Sci. Technol. A **4**, 2024 (1986) find at $T=80$ K $b \simeq 0.15$ eV; a higher value of ~ 0.45 eV is found at 300 K.

[47]J. C. Brice, in *Properties of Mercury Cadmium Telluride, Data Review Series,* edited by J. Brice and P. Capper (The Institute of Electrical Engineers, London, 1987), p. 103, give at low temperature $b=0.23$ eV for $Hg_{0.5}Cd_{0.5}Te$. However, G. L. Hansen, J. L. Schmidt and T. N. Casselman, J. Appl. Phys. **53**, 7099 (1982), give at $T=0$ K $b(Hg_{0.5}Cd_{0.5}Te)=0.44$ eV.

[48]K. C. Hass, H. Ehrenreich, and B. Velický, Phys. Rev. B **27**, 1088 (1983).

[49]M. A. Berding, S. Krishnamurthy, A. Sher, and A.-B. Chen, J. Vac. Sci. Technol. A **5**, 3014 (1987).

[50]S.-H. Wei and A. Zunger, J. Vac. Sci. Technol. A **6**, 2597 (1988).

[51](a) S.-H. Wei and A. Zunger, Phys. Rev. B **39**, 3279 (1989); J. E. Bernard and A. Zunger, *ibid.* **36**, 3199 (1987); (b) For example, using the SQS-4 structure we find that structural relaxation *reduces* the direct band gap by $\Delta E = -0.005$ eV. This is in contrast with the increase of small $\Delta E = +0.013$ eV obtained by Lempert and co-workers in Ref. 32, where $\Delta E = E_g(\text{M-CPA}) - E_g(\text{S-CPA})$ was used.

[52]C. K. Shih, W. E. Spicer, J. K. Furdyna, and A. Sher, J. Vac. Sci. Technol. A **5**, 3031 (1987).

[53]W. E. Spicer, J. A. Silberman, I. Lindau, A.-B. Chen, A. Sher, and J. A. Wilson, J. Vac. Sci. Technol. A **1**, 1735 (1983).

[54]A.-B. Chen and A. Sher, J. Vac. Sci. Technol. **21**, 138 (1982).

[55]K. C. Hass and H. Ehrenreich, J. Vac. Sci. Technol. A **1**, 1678 (1983).

[56]H. Ehrenreich and K. C. Hass, J. Vac. Sci. Technol. **21**, 133 (1982).

[57]J. Kudrnovsky, V. Drchal, M. Sob, N. E. Christensen, and O. K. Andersen, Phys. Rev. B **40**, 10 029 (1989).

[58]J. Kudrnovksy and V. Drchal, Phys. Rev. B **41**, 7515 (1990).

[59]These are the spin-orbit splittings calculated at point Γ. If we calculate Δ_d from the DOS given in Fig. 2, we would obtain 0.34, 0.67, and 1.80 eV, for ZnTe, CdTe, and HgTe, respectively.

[60]W. A. Harrison, *Electronic Structure and the Properties of Solids* (Freeman, San Francisco, 1980).